Received: 10 January 2025 | Revised: 16 May 2025 | Accepted: 27 May 2025

DOI: 10.1002/esp.70106

LETTER TO ESEX

ESPL WILEY

Potential and constraints of uncrewed aerial vehicle orthoimagery for rivers: A direct comparison with field measurements for mapping boulders

Christopher Wård | Richard J. Mason | Ricardo Carrillo | Lina E. Polvi

Department of Ecology, Environment and Geoscience, Linnaeus väg 6, Umeå University, Umeå, Sweden

Correspondence
Richard J. Mason, Department of Ecology, Environment and Geoscience, Linnaeus väg 6, Umeå University, S-907 36, Umeå, Sweden.
Email: richard.mason@umu.se

Funding information
Svenska Forskningsrådet Formas, Grant/Award Number: 2014-00484; Swedish Agency for Marine and Water Management

Abstract

Technological advances continue to improve our ability to detect landforms and landscape changes. Remote sensing can provide geomorphological information at larger scales than previously possible but interpreting this information can be more challenging than for field data. Measuring and mapping roughness elements, such as boulders and large wood, is essential for understanding geomorphic processes and restoration in many landscapes where these are abundant. Mapping roughness elements from aerial orthoimagery is common but could produce different results than field measurements due to the 2D nature of the imagery and the variable ability to detect boulders through water and vegetation. We compared measurements of river boulders from aerial imagery collected by uncrewed aerial vehicles (UAVs) to direct measurements in the field. We surveyed boulder size, density and spatial distributions using both approaches at eight river reaches in northern Sweden. We found that the density, coverage and size of boulders mapped from UAVs were strongly correlated with those from field measurements, giving confidence in UAV methods. However, the UAV approach consistently resulted in fewer boulders (30% lower density), lower boulder coverage and smaller boulders (7% smaller mean b-axis) compared to field measurements. The difference between field and UAV measurements was strongly associated with river bankfull depth. Therefore, we conclude that UAV measurements should be restricted to sites with low depth or high visibility through the water column and where bias in boulder detection with depth is not likely to influence study conclusions. In reaches with many boulders, overlap of boulders also likely reduces the suitability of aerial imagery. We conclude that aerial imagery has high potential for mapping landforms in rivers but is not directly equivalent to field studies and the implications of hiding by water, sediment and vegetation need to be considered.

KEYWORDS
boulders, drone, remote sensing, river restoration, UAV

1 | INTRODUCTION

Technological advances continue to improve our ability to detect landforms and landscape changes (Viles, 2016), and traditional field surveys are increasingly replaced, or complemented by, remote sensing. Remotely collected data, including aerial imagery from satellites or uncrewed aerial vehicles (UAVs) and Light Detection And Ranging (LiDAR), provide new insights into earth surface processes at previously impossible scales due to faster data collection and the opportunity to survey inaccessible sites (e.g. other planets, Mangold et al., 2021). However, whilst a wealth of geomorphological information is stored in remotely sensed products, extracting and interpreting this information can be challenging (Brasington et al., 2012).

The field of fluvial geomorphology has benefitted from remote surveying techniques, now commonly used to map river landforms and ecology (Acharya et al., 2021; Rivas Casado et al., 2017; Rusnák et al., 2018; Woellner & Wagner, 2019). In particular, advances in UAV technology have increased UAV accessibility, allowing both scientists and land managers to easily collect and analyse UAV imagery. For example, river restoration practitioners widely use UAV imagery to assess and communicate hydromorphological changes (Langhammer, 2019; Williams et al., 2020; Woodget et al., 2017).

Boulders are important features in many landscapes, influencing geomorphic, hydrological and ecological processes (Causon Deguara et al., 2023; Nativ et al., 2022; Pérez-Alberti & Trenhaile, 2015; Sakamoto & Gomez, 2019). For example, boulders provide roughness that controls river slope, width (Montgomery & Buffington, 1997; Nativ et al., 2022) and the distribution of in-channel habitats (Papanicolaou et al., 2018). However, anthropogenic modification of rivers has often involved the removal of these roughness elements (Korpak, 2017; Wohl, 2019), and restoration is now attempting to replace them because of their positive influence on habitat complexity. Both management and scientific study of boulder-bed rivers require measuring and mapping these roughness elements (Golpira et al., 2022; Lee & Ferguson, 2002; Mason & Polvi, 2023; Nilsson et al., 2015; Wiener & Pasternack, 2022).

Direct field mapping using a GPS, total station or tape measure (e.g. Mason & Polvi, 2023), is time-consuming, especially in areas with high boulder densities (e.g. 100–1000 s of boulders/ha; Nativ et al., 2022; Wiener & Pasternack, 2022; Sakamoto & Gomez, 2019). Remote sensing may provide the opportunity to measure boulders, large wood and other roughness elements at larger scales, in inaccessible locations, and with less effort than traditional field techniques.

A wide variety of technologies can be used to map individual particles. 3D models built from LiDAR or structure-from-motion (SfM) have been used to map boulders (Resop et al., 2012) and quantify particle size distributions (e.g. Chen et al., 2019). For example, Wiener and Pasternack (2022) used aerial LiDAR to automate identification of boulders and bedrock elements. However, without commissioned flights, widely available LiDAR is usually too sparse (e.g. typically 0.5–3-m resolution for well-mapped regions and considerably less across much of the globe; Hancock et al., 2021), and 3D models in rivers frequently require some ground-based data collection (Rusnák et al., 2018). Therefore, whilst a wealth of information is available in 3D models of rivers, such data are expensive and time-consuming to collect, often requiring field validation or georeferencing, and the analysis is computationally intensive, all partially negating the advantages of remote techniques.

In contrast, high-resolution 2D imagery of river environments is widely available, enabling measurement of particle sizes (Buscombe et al., 2010; Graham et al., 2005; Lang et al., 2021; Marchetti et al., 2022). Using aerial imagery, the resolution is frequently insufficient to map the full grain-size distribution (Carbonneau et al., 2004), but large roughness elements can still be identified. Thus, studies using satellite (e.g. Finnegan et al., 2019) and UAV orthoimagery (e.g. Nativ et al., 2022) have demonstrated the advantages of aerial imagery for boulder mapping (Causon Deguara et al., 2023; Nativ et al., 2022; Sakamoto & Gomez, 2019; Wiener & Pasternack, 2022).

However, measuring river boulders from aerial imagery presents challenges. Boulders are frequently abundant and may be hidden by other particles, water and vegetation. In a terrestrial setting, Causon Deguara et al. (2023) compared boulder dimensions derived from UAV models to the same data collected via direct measurements in the field, finding a generally good match between the techniques (for a- and b-axes). However, unlike terrestrial boulder measurements, in rivers, water restricts the ability to detect boulders, and riparian or in-channel vegetation may also obscure boulders. Furthermore, orthoimagery methods only have the possibility to measure boulders in two dimensions, lacking information on boulder height (Wiener & Pasternack, 2022). Consequently, there are many reasons to hypothesise that boulder measurements from aerial imagery would differ from traditional field measurements. Understanding these differences and the advantages and disadvantages of each approach is important to evaluate the consequences and potential biases of UAV or field measurements and to compare between techniques, for mapping boulders or other landforms in river settings.

In this article, we compare measurements of river boulders from aerial orthoimagery collected by UAVs to direct measurements in the field. We investigate boulder measurement in semi-alluvial rivers in northern Sweden flowing through glacially or meltwater-deposited boulder fields (Mason & Polvi, 2023). Humans have removed boulders from most Swedish streams to provide float pathways for timber (Törnlund & Östlund, 2006). Timber-floating ended in the 1970s–1980s, and subsequent restoration efforts have replaced river boulders, because of their hydromorphological and ecological importance (Nilsson et al., 2005). Understanding the density, spatial distribution and characteristics of boulders is therefore important to ensure restoration recreates appropriate river morphology and habitats. Mapping boulder distributions is also important to understand pre-disturbance fluvial processes. In a study mapping river boulders at sites with low human disturbance, Mason and Polvi (2023) concluded that river morphology is primarily driven by glacial legacy boulders and till landforms, with limited fluvial influence. They also found little self-organisation between channel morphology or catchment area and the degree of boulder influence but reported positive associations between boulder density, coverage, protrusion and depth.

In this study, we ask how and why do measures of boulders from UAV-derived orthoimagery and direct field measurements differ? We also investigate whether mapping boulders by UAV rather than in the field would change the conclusions of Mason and Polvi (2023) on controls on boulder-bed channel morphology in northern Sweden.

2 | METHODS AND DATA ANALYSIS

We surveyed eight reaches (75–100-m length) in northern Sweden (Figure 1). Reaches were selected for a previous study to determine hydromorphological controls on semi-alluvial channel morphology (Mason & Polvi, 2023). Studied reaches are believed to be without direct anthropogenic impact to their morphology and boulder distributions, based on local historical knowledge and visual field inspection. The eight study reaches varied in catchment size from 11 to 82 km^2 and channel width from 5 to 25 m. The surveyed areas ranged from 570 to 2450 m^2, and the reach slope ranged from 0.9% to 4.7%. One field survey (Reach 2) was conducted in August 2020, the others in

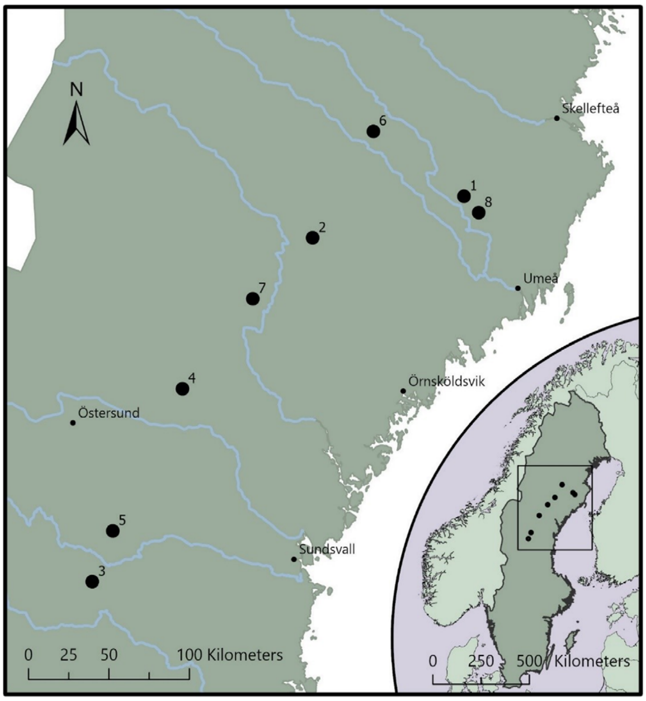

FIGURE 1 Locations of the eight study reaches in northern Sweden. Major rivers (in blue) and major cities shown.

October 2020. Field mapping of boulders was conducted for Reach 6 in 2017 and updated in October 2020 to ensure consistency with the other reaches and the UAV flight. UAV flights were conducted at the same time as field measurements except for Reach 2, which was flown in October. We defined boulders as having a minimum b-axis of 1 m and compared the results from UAV imagery and field measurements.

2.1 | Field measurements

The field surveys were conducted to map reach morphology, sediment size distribution, in-channel boulders and large wood (for further details, see Mason & Polvi, 2023). We mapped the channel bankfull edge using a Trimble S3 total station. All islands larger than 1 m^2 were mapped and subtracted from the bankfull area. In addition, we measured five equally spaced channel cross-sections recording both water elevation at the time of survey and the bankfull elevation. We surveyed the longitudinal profile to calculate reach bed slope. The particle size distribution was measured using a 200-particle grid count over the reach area (Green, 2003).

For all boulders in the reach that were either protruding above the water surface or completely under the surface, we mapped three locations with the total station: (1) the highest point, (2) the river bed elevation adjacent to the upstream edge of the boulder and (3) the river bed elevation directly downstream of the boulder. We also identified and measured the boulder b-axis using a 2-m ruler. We defined the b-axis as the largest diameter perpendicular to the a-axis (the longest axis). From these field measurements, boulder centre was calculated as the midpoint between the upstream and downstream measurements. Protrusion was calculated as the difference in elevation between the boulder top and the mean of the upstream and downstream measurements. Further analyses were identical for field and UAV-based data and are detailed in Section 2.3.

2.2 | UAV measurements

Aerial images were captured using a DJI Phantom Pro UAV (FC6310R camera with 8.8-mm focal length and 20-MP sensor). The survey was conducted manually following the centre of the river without any planning software, capturing images both nadir to the ground and angled. Flight heights were a compromise between pixel resolution at the ground and spatial coverage, whilst staying above the tree height. In some reaches, images were collected at multiple elevations to get a broader view of the reach. Lower elevations range from 27 to 60 m, and higher elevations range from 45 to 125 m (Table 1). We used Agisoft Metashape Professional (version 2.0.3) to align the images, scale the model and generate orthomosaics. Since ground control points were not collected in the field, known distances in the images (e.g. the length and width of fully visible large wood pieces from the field survey; Section 2.1) were used to scale the images and check the measures (check bars) using the scale bar tool in Metashape. A dense point cloud was created and manually filtered to remove anomalous points in the channel. From this, a digital elevation model was built and used to generate the orthomosaic. Where tree coverage obscured portions of the channel in the orthoimagery, we selected images for use in the orthomosaic that maximised channel visibility. The final pixel size in the orthomosaics varied between 6.29 and 20.02 mm (Table 1).

The scale and check bars used to scale the models and determine errors are measured in 3D, whilst our orthomosaics are 2D. To assess error in 2D (x and y), we extracted the observed and estimated coordinates from the check bar end points, after tie point alignment and camera optimisation in Metashape. We then calculated the linear distances of the check bars using the x- and y-coordinates and determined the error between observed and estimated distances. The error was scaled by dividing by the observed distance to non-dimensionalise the error (James et al., 2019). We calculated systematic error (accuracy) as mean error (ME) and mean absolute error (MAE), while random error (precision) was calculated with standard deviation of the errors (SDE). Since we lacked GCPs, we were not able to eliminate systematic error, but random error was reduced using the Sparse Cloud Cleaning (SCC) script (Mohren & Schulze, 2024). With systematic and random errors, we computed total uncertainty with ME and total uncertainty with tj MAE using the root-sum-squared method. We also computed root mean squared errors to compare the result with the total uncertainty values. The results of the different types of errors are presented in Table 1 and Figure 2a. In order to be more conservative in the propagation of the measurement error and its influence on boulder counts from the orthomosaic, we use the larger total uncertainty, calculated with the MAE.

Within the bankfull channel margins, as defined from the field mapping, we manually digitised the centre point of all visible boulders above the threshold of 1 m for the visible b-axis (Figure 3). Since the imagery is 2D, the b-axis measured in the UAV imagery assumes that the a- and b-axes are visible, and the c-axis is vertical. For boulders along the channel edge, any boulder that was partly within the channel area was included. We also digitised the channel area obscured by riparian vegetation.

TABLE 1 UAV flight surveys and processing summary, including final error and image resolution.

Reach number	Number of images	Flight mean altitude (m)	Total scale bars	Control scale bars	Check scale bars	Pixel resolution (mm)	Mean error (ME)	Mean absolute error (MAE)	Standard deviation (SDE)	Root mean squared error (RMSE)	Total uncertainty (ME + SDE)	Total absolute uncertainty (MAE + SDE)
1	22	27	9	5	4	7.36	0.066	0.137	0.195	0.182	0.206	0.238
2	35	20/45	14	7	7	9.87	0.042	0.042	0.052	0.064	0.067	0.067
3	27	42/125	5	3	2	20.02	−0.017	0.017	0.012	0.019	0.021	0.021
4	12	55	9	5	4	10.59	0.027	0.052	0.057	0.057	0.063	0.078
5	38	35/105	9	5	4	10.15	0.008	0.008	0.002	0.008	0.008	0.008
6	15	60	6	3	3	10.69	−0.150	0.150	0.189	0.215	0.241	0.241
7	41	30	6	3	3	8.48	0.009	0.079	0.100	0.082	0.100	0.127
8	30	23	11	6	5	6.29	−0.032	0.079	0.139	0.128	0.143	0.160

2.3 | Boulder comparisons

For both boulder measurement techniques, boulders and reach maps were processed in ArcGIS Pro. The ability to measure boulder surface coverage (at least above the water surface) is an advantage of aerial imagery but would be prohibitively labour intensive in the field; therefore, we simplified boulders to circles in order to directly compare the two techniques. Boulder circles were centred on measured centre points (from orthomosaics or total station) with diameters equal to measured boulder b-axis. Boulder coverage was estimated by summing the area of boulders without double-counting overlapping areas and excluding portions of boulders outside of the bankfull channel margin, to provide a percentage of the channel covered by boulders. The total number of boulders, boulder density (boulders per m^2) and mean boulder b-axis were also calculated.

To understand and control for the error associated with the orthomosaic imagery, we estimated the error propagated from each image (in m m^{-1}) to boulder measurements. We did this using the grain-size distribution measurements from each reach, to calculate how many extra or fewer grains would be classified as boulders if the images were scaled smaller or larger than reality. Using the total uncertainty calculated with MAE and SD for each site, we calculated the percentage of particles in the grain-size distribution within the uncertainty range of the 1-m definition and applied these percentages to the measured boulders. This resulted in an estimate of how the number of measured boulders would differ due to image scaling errors (Figure 2b).

To compare the two boulder-measurement techniques, we conducted paired *t*-tests and correlation analyses for boulder density, boulder coverage and mean b-axis. To understand why the techniques might differ, we used linear regressions between the percentage difference between the measured results and six potential explanatory variables: mean bankfull channel depth, mean water depth, drainage area (as a proxy for discharge), vegetation coverage, D_{84} and mean river width. Last, we compared associations between reach boulder characteristics and other reach characteristics to determine if the choice of boulder-measurement technique would change our understanding of hydromorphological functioning of rivers in northern Sweden, as determined by Mason and Polvi (2023). These were compared using Pearson's correlation analyses. For all statistical tests, we give more confidence to associations significant at the $p < 0.05$ level but also discuss those significant at $p < 0.1$ level, since they may indicate underlying processes of interest, which might be significant at the 0.05 level if more sites were considered. All statistics were performed in R Studio version 4.1.3.

3 | RESULTS

The number of boulders ranged from 8 to 324 detected from the UAV orthomosaics and from 8 to 524 measured in the field (Table 2). All but one reach (Reach 8) had lower boulder density, area and coverage with the UAV data than the field data. Site 8 only had eight boulders with both techniques but still had a decrease in boulder coverage from 1.8% to 1.3% of channel area covered by boulders (−28.5%) (Table 2). The mean decrease for all eight study reaches was 34% ± 22% for boulder density and 33% ± 15% for boulder coverage

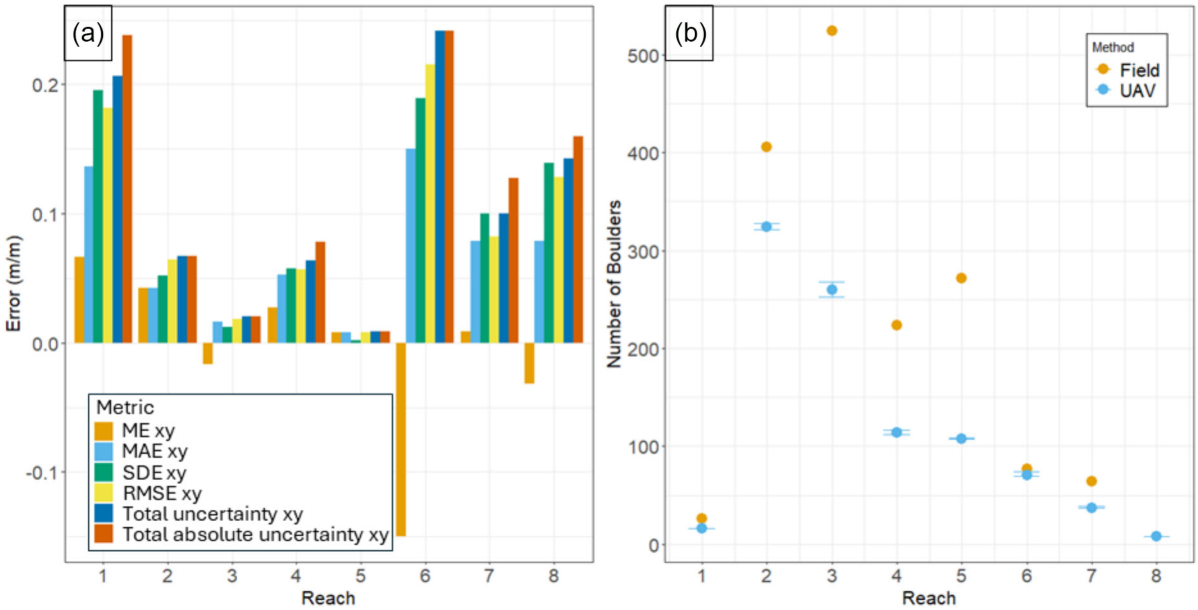

FIGURE 2 Orthomosaic errors for each studied river reach. (a) Total error and individual errors for each reach (described in text). (b) Influence of orthomosaic error on boulder counts across all river reaches. Field error was not quantified.

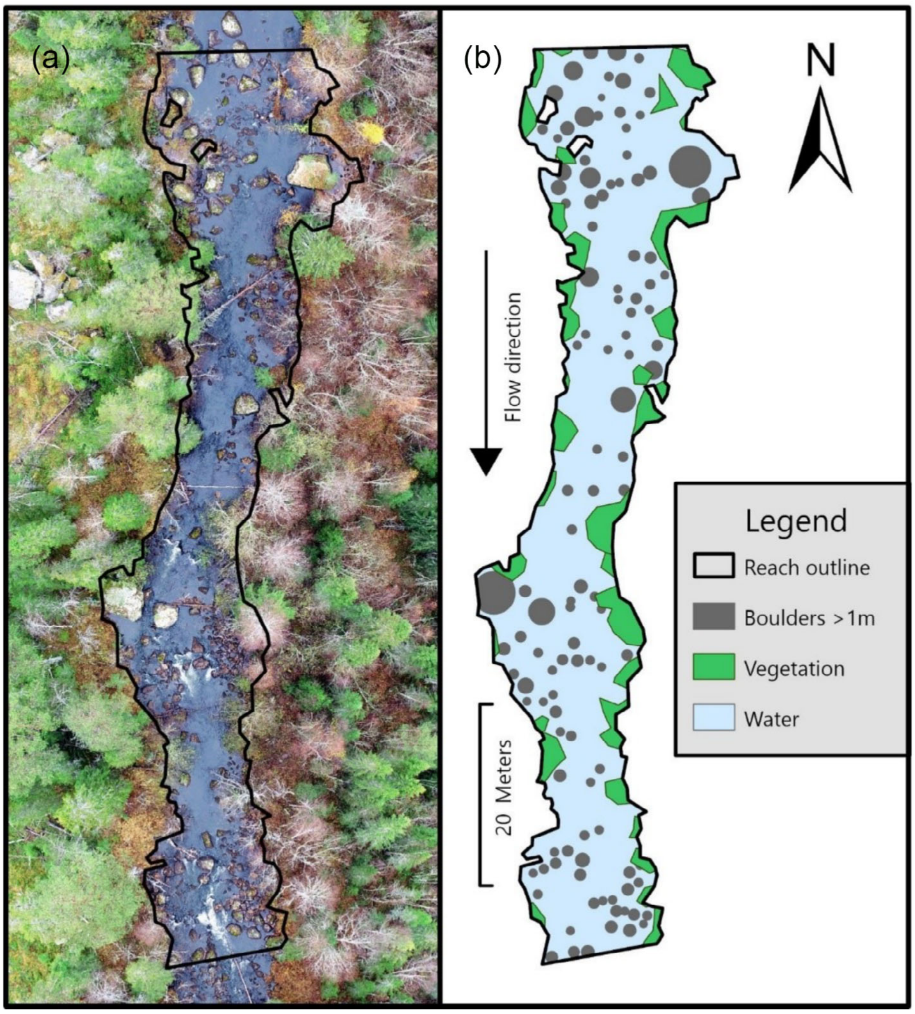

FIGURE 3 Example of study reach digitization from UAV imagery (study reach number 4, Länglingsjön). (a) UAV-derived orthomosaic with channel area within bankfull (reach outline in black). (b) Channel area within bankfull with UAV-digitised boulders in grey and vegetation in green. Boulder diameters are equal to the b-axis.

TABLE 2 Boulder metric data for all eight study sites from UAV data and field data. Mean and standard deviation shown for boulder metrics for both UAV and field data.

Boulder metrics	Unit	Study reach 1	2	3	4	5	6	7	8	Mean	SD
Boulders >1 m (Field)	-	26	406	524	224	272	77	64	8	200	190
Boulders >1 m (UAV)	-	16	324	260	114	108	71	37	8	117	116
Boulder density (Field)	m^{-2}	0.04	0.17	0.43	0.17	0.29	0.10	0.11	0.01	0.17	0.14
Boulder density (UAV)	m^{-2}	0.02	0.13	0.21	0.09	0.11	0.09	0.06	0.01	0.09	0.06
Change in boulder density (UAV-field)	%	−38	−20	−50	−49	−60	−8	−42	0	−34	22
Boulder area (Field)	m^2	22	701	702	351	357	112	82	10	292	286
Boulder area (UAV)	m^2	14	613	406	196	157	98	57	7	194	213
Boulder coverage (Field)	%	3	29	57	27	38	15	14	2	23	19
Boulder coverage (UAV)	%	2	25	33	15	17	13	10	1	15	11
Change in boulder coverage (UAV-field)	%	−35	−13	−42	−44	−56	−12	−30	−29	−33	15

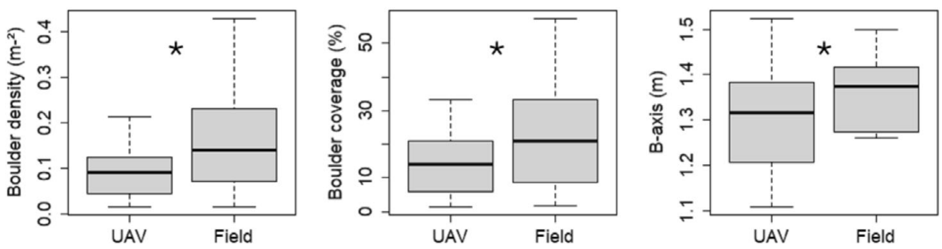

FIGURE 4 Boxplots comparing UAV and field data for three boulder metrics. The line represents the median, the box represents the interquartile range, and the whiskers represent the minimum and maximum values. The difference between UAV data and field data was significant for all boulder metrics (paired *t*-test, $p < 0.05$).

(Table 2; Figure 4). Mean boulder b-axis also decreased from 1.4 ± 0.5 m to 1.3 ± 0.4 m (7% decrease). The paired *t*-tests showed that UAV-measured boulders resulted in fewer boulders ($p = 0.040$), lower coverage ($p = 0.037$) and smaller boulders ($p = 0.031$) than field measurements (Figure 4). However, there was a strong positive correlation between UAV-measured and field-measured boulder metrics (boulder density, coverage and b-axis values) across all reaches (Figure 5).

Evaluating the controls on the difference between UAV and field data (Figure 6), mean bankfull depth showed significant linear correlations with percent difference for both boulder density and boulder coverage ($p = 0.019$ and $p = 0.042$, respectively) (Figure 6a,g). Mean water depth was significantly positively correlated with percent difference in boulder coverage ($p = 0.014$). Similarly, mean water depth had a positive correlation with percent difference in boulder coverage, which was significant at the $p < 0.1$ level ($p = 0.0503$; Figure 6b,h). Neither drainage area nor vegetation coverage was correlated with percent difference in boulder density or boulder coverage (Figure 6c,d,i,j, $p > 0.1$). D_{84} was significantly correlated with the difference in boulder density at the $p < 0.1$ level ($p = 0.051$), but boulder coverage was not significant ($p = 0.18$) (Figure 6e,k). Mean width was also not correlated with the difference in boulder density ($p = 0.91$) or boulder coverage ($p = 0.51$) (Figure 6f,l).

We also checked to see if uncertainty of the orthomosaic images used for boulder measurements could explain the differences between field and UAV results. The total uncertainty based on systematic and random errors (MAE and SDE, respectively) obtained from image processing in Agisoft Metashape ranged from 0.008 to 0.241 m m^{-1}. The uncertainty of each image does not explain differences in either boulder density or boulder coverage, showing no relationship between the variables (slope statistically equal to zero; Figure 7).

Last, we compared associations between reach boulder metrics and other reach characteristics to determine if the choice of boulder-measurement technique would affect results of an analysis of controls on river boulder metrics in northern Sweden. We found that UAV and field data showed broadly the same direction of correlations with reach and catchment scale variables, but the magnitude of the correlation was much lower for UAV-measured than field-measured boulders (Figure 8). Analysis of the slopes of all six associations shows a mean twofold greater relationship in the field measurements compared to UAV measurements (mean proportion = 2.13, SD = 0.18).

4 | DISCUSSION

4.1 | How and why do boulder measurements differ between UAV and field data?

Boulder metrics measured in the field and with UAV were strongly correlated (Figure 5), and therefore, for many studies, UAVs likely

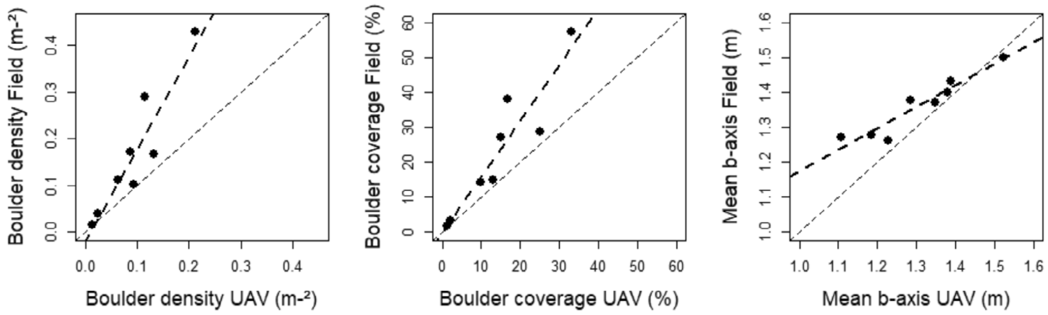

FIGURE 5 Correlations between boulder metrics (density, coverage and mean b-axis) between boulder measurements conducted in the field and using UAV imagery. Grey dotted line shows 1:1 association, bold black dashed line is the linear trend line.

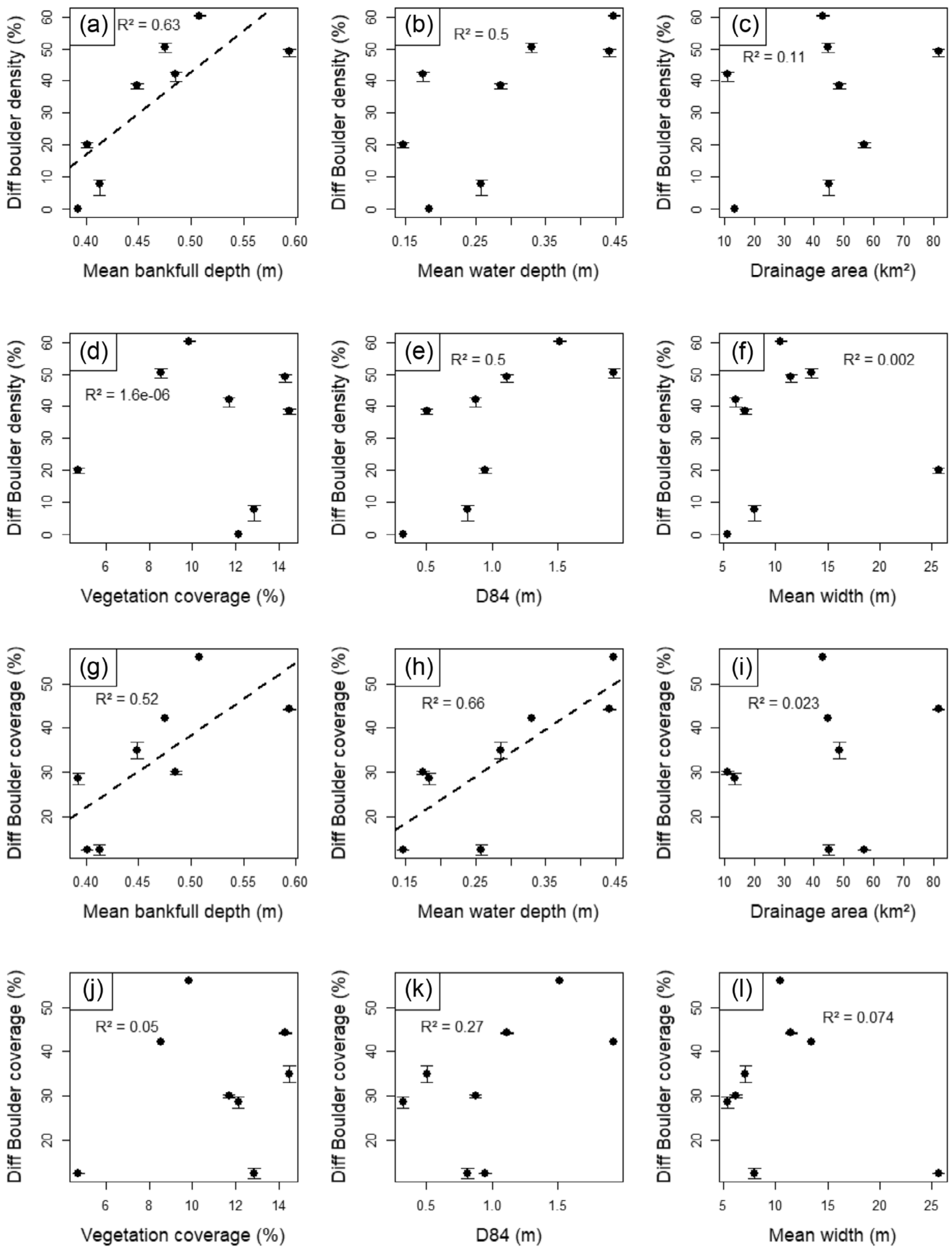

FIGURE 6 Comparing the influence of UAV versus field measurements on boulder density and coverage correlations with catchment- and reach-scale characteristics as explanatory variables. R^2 values displayed, and all significant ($p < 0.05$) correlations are shown with linear trend line. Error bars are derived from an estimate of error propagated from image error (±m m^{-1}) using the grain-size distribution (see section 2.5).

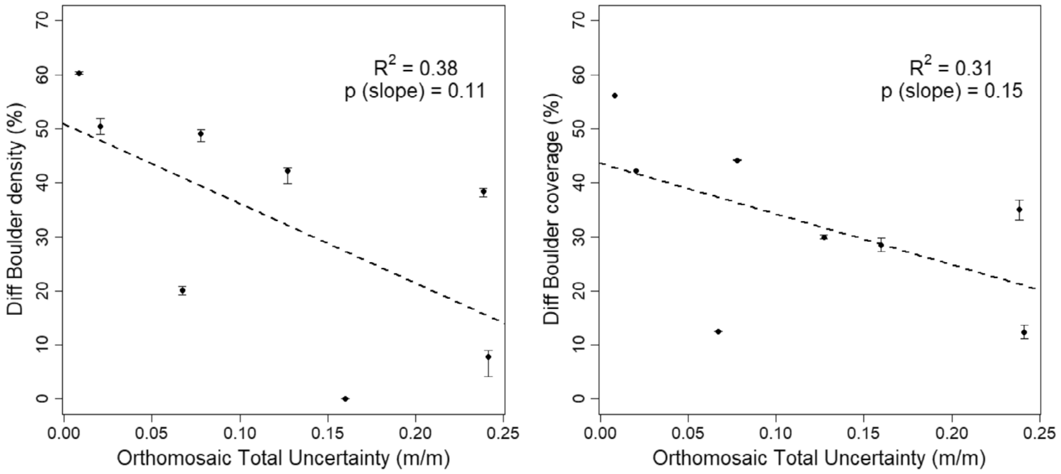

FIGURE 7 Scatter plots of linear regressions between difference in boulder density and boulder coverage between UAV and field data and orthomosaic total uncertainty (MAE + SDE). Both slopes are not significantly different to zero ($p < 0.05$).

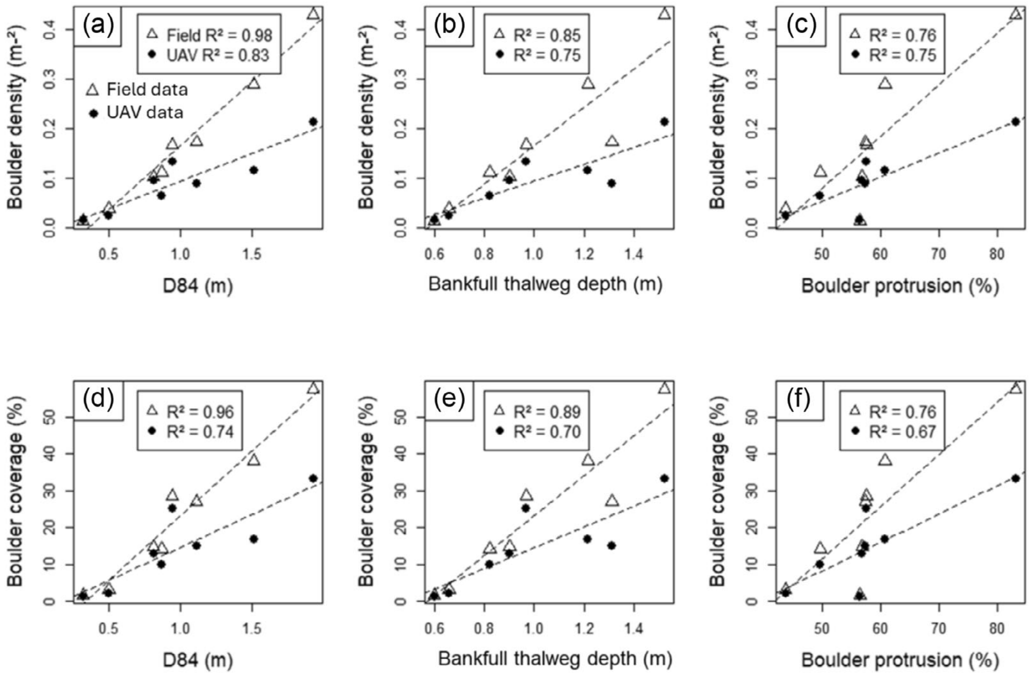

FIGURE 8 Associations between boulder metrics (density and coverage) and reach-scale characteristics, D_{84}, mean bankfull thalweg depth and protrusion. All correlations shown were significant ($p < 0.05$).

provide a quicker and more efficient alternative to field boulder mapping. However, UAV orthophotos also yielded consistently lower boulder density, boulder coverage and mean b-axis (34%, 32% and 7% lower, respectively; Figure 4). Explaining these differences is important to identify potential biases and evaluate the opportunities and challenges with each technique. We hypothesised that boulder orientation and interaction with other particles, hiding by water and vegetation and error in the orthomosaic generation, might explain differences between UAV and field mapping. In addition to completely hiding boulders from view, these factors could affect measured particle size and coverage. For example, at site eight, the number of boulders measured was the same for both techniques (8), but boulder area was lower for the UAV (Table 2).

4.1.1 | Orientation and other particles

A fundamental difference between the two measurement techniques is the 2D nature of aerial imagery. In the field, all three axes of the boulder could be measured, but with UAV only two axes can be measured, and we cannot know which axes these are. We therefore assume that visible axes are *a* and *b* and that the *c*-axis is orientated vertically. Sediment particles are most stable with c-axes vertical; however, interactions with other particles, such as imbrication and clustering, often cause particles to settle in other orientations (Church et al., 1987; Hodge et al., 2009; Rust, 1972). Furthermore, previous research in these streams has suggested that these boulders have not been fluvially sorted since deposited by (de)glaciation processes

(Mason & Polvi, 2023); thus, they may not have experienced sufficient energy to organise to such a stable state. Therefore, the assumption of a vertical c-axis may not to be true for many boulders.

As a result, UAV measurements likely underestimate the true size of boulders since if either the a- or b-axis was vertical, we would incorrectly assume the c-axis is the b-axis and define boulders accordingly. UAV measurements also assume that particle axes are orientated orthogonal and perpendicular to the horizontal, whereas in the field, the particle axes can be evaluated at any angle. Therefore, orientation could explain some of the difference between UAV and field boulder metrics. We were not able to more fully evaluate this from our data since we did not record the orientation of each axis in the field.

A further possible cause for differences between UAV and field boulder measurements is the hiding of all or part of boulders under other boulders. Many rivers had overlapping boulders. The difference in boulder density between the two measurements was correlated with reach D84 (although this was not significant; Figure 6e), perhaps indicating that more and larger boulders reduce the ability of UAVs to measure boulders.

4.1.2 | Obscured by water

The ability to map boulders below the water surface from UAV-based photography is limited (Wiener & Pasternack, 2022) and dependent on the visibility though the water. If the water is clear and the surface smooth, then detecting landforms is possible (Woodget et al., 2015) although refraction could alter apparent boulder size. However, turbulence or turbidity can restrict visibility or make it entirely impossible to see any boulders beneath the surface. In this study, there was varying visibility between the study sites. Dissolved organic carbon leading to 'browning' of boreal streams (Kritzberg et al., 2020) made visibility below the surface in our studied streams especially poor. In total, only a few totally submerged boulders were measured (<10 across all sites), and at three sites, there was no visibility below the water surface whatsoever. The difference in boulder density and coverage between UAV and field data was associated with bankfull and mean depth (Figure 6). This suggests that deeper water results in fewer boulders and a smaller total boulder area measured by UAV (Figure 9). Deeper and faster flowing water also likely reduces the efficiency of boulder detection in the field. However, since extra care was taken to search these areas under water, the effect will be much less significant than for UAV imagery.

4.1.3 | Obscured by vegetation

A further expected disadvantage of UAV measurements of boulders was vegetation cover. The studied river reaches were all bordered by riparian birch, pine and spruce forests. However, the proportion of the channel obscured by riparian vegetation was typically low (5%–14%) and showed no association with the difference between UAV and field measures, suggesting that this was not an important factor. The orthomosaics were carefully modified to provide the best view of the channel. In future studies, angled UAV images might further improve visibility.

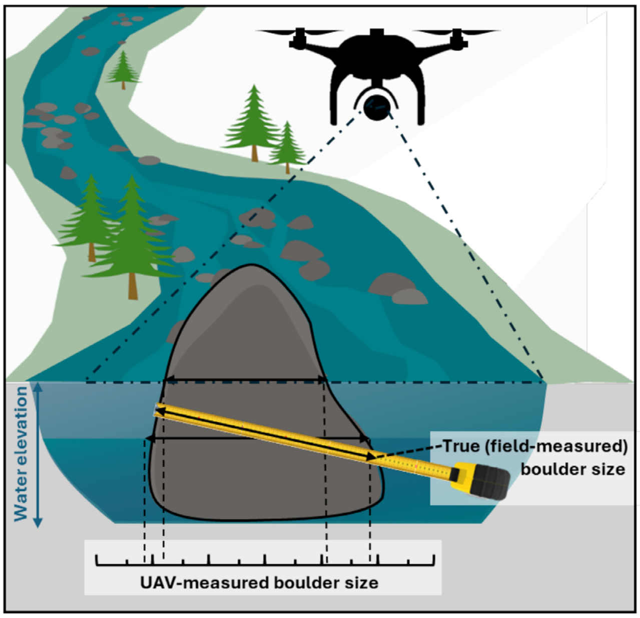

FIGURE 9 Conceptual summary of key differences in boulder measurement from field versus UAV surveys. Particle visibility above water surface is a key control on the accuracy of UAV measurements. Particle orientation, obstruction by other particles and vegetation may also influence the comparison.

4.1.4 | UAV orthomosaic errors

Finally, a hypothesised reason for the difference between the two methods was the error in the orthomosaic imagery. Using scale bars rather than surveyed targets, increased the error of our orthomosaics. However, this was also not associated with the differences in boulder measurements (Figure 7). Whilst there is a possibility that some boulders were missed or included due to the distortion of the orthomosaic, other factors (e.g. water) were more important for the difference in estimates in this study. As the threshold of boulder size decreases (<1 m), image quality becomes more important as the boulder size approaches the image error. Both RTK-UAV or ground control points would further reduce these errors (e.g. from 7 cm to less than 2 cm; Gómez-Gutiérrez et al., 2024). Using RTK-UAV rather than ground control points would vastly increase survey speed and the ability to use UAV boulder measurement in locations without field access.

4.2 | Can UAVs replace field surveys?

Future studies should appreciate the advantages and disadvantages of each before choosing a measurement technique (Table 3). It is evident that both aerial imagery from UAV and field-based boulder measurements captured the relative differences in boulder metrics between the sites (Figure 5). Consequently, we concur with Mason and Polvi (2023) that a positive association exists between reach bankfull thalweg depth and boulder density (and concentration; Figure 8b & e). This may indicate fluvial adjustment of depth to glacial legacy boulders. However, correlations between boulder metrics and reach characteristics were all weaker for UAV than field data, and there is therefore a risk that studies relying on orthoimagery will not detect

TABLE 3 Advantages and disadvantages of field- and UAV-based measurements of river boulders.

Factor	Field	UAV-based orthoimagery
Measured boulder properties	Can identify and measure true a-, b- and c-axes and protrusion.	Can only measure boulder properties visible from above, horizontal axis. Can easily measure exposed areas of boulders from above.
Time and survey size trade-off	Time-consuming in the field. About 16 h for one 100-m reach. Processing of field data and creation of boulder maps conducted in the lab (about 1 h per site).	<1 h per 100-m site. More if control points are used. Digitising of orthoimages is required in the lab (about 2 h per site).
Precision	Precision is very high with ruler and/or total station. Precision is lower but still high with RTK GPS.	Low—no RTK Medium—RTK High—RTK + ground control points
Sensitivity to environmental constraints	Less sensitive to obstructions by water since surveyor can measure under water. Tree coverage has little influence on measurements except to determine whether GPS or total station are employed. Field surveys are more vulnerable to surveyor subjectivity, which could vary with weather conditions.	Very sensitive to obstruction by water, vegetation or other boulders. Therefore, best conducted during low flow conditions but can also provide measurements in high flows when unsafe to access. Cannot fly in bad weather (heavy wind or precipitation) Lower risk to surveyors

patterns that would require the extra information on boulder distributions revealed by field surveys.

Since aerial imagery can only provide information on visible elements of particles, they will differ from field measurements since not all particle axes can be measured. However, classification of boulders by the b-axis, common in field studies, can also be arbitrary (Mason & Polvi, 2024), so this is not a problematic limitation of UAVs for most studies. However, water elevation was found to be a key control on the difference between UAV and field measures. Poor visibility of boulders is potentially problematic for studies which compare boulder distributions among reaches, or within a reach, across which visibility might vary. For example, this could lead to false conclusions of fewer boulders in deeper (i.e. thalwegs or pools) or higher velocity water (due to surface disturbance). For studies on boulder spatial distributions, (e.g. Mason & Polvi, 2023), this could lead to biased results since pools upstream of boulder steps could hide boulders leading to false conclusions of boulder clustering. Furthermore, at sites with extensive vegetation or hiding by other boulders, field measurement may be preferable.

An advantage of orthoimagery over field measurements is the ability to map more accurately boulder coverage in the horizontal dimension, although this comes at the expense of information in the vertical dimension. Although we could not compare aerial coverage mapping of boulders to our field techniques, as our measurements needed to be directly comparable, we mapped boulders using both methods at one site (Figure 10). We found that mapping boulders as circles according to b-axis accounted for 86% of the total surface coverage. Whether this additional detail is informative depends on the research question, but it still does not reduce uncertainties arising due to water coverage, particle orientation, protrusion or obstruction by other boulders.

Whilst we focussed on boulders, our comparison applies to other uses of aerial imagery. Our findings would also apply to satellite imagery, which offers unparalleled spatial and temporal scales for environmental analysis (Tomsett & Leyland, 2019). With increasing availability and use of remote techniques it is important to evaluate how they differ from field techniques. Whilst there is research comparing the suitability of different remote sensing techniques (e.g. Nikolakopoulos et al., 2023; Siewert & Olofsson, 2020), there are surprisingly few comparisons with field surveys. Bangen et al. (2014) compared aerial LiDAR to total station and RTK GPS surveys of topography. Both water and vegetation were challenges for LiDAR in this study, due to signal scattering and attenuation.

Many of the differences between UAV and field boulder measurements would be reduced if 3D topographic data were available, rather than 2D orthoimagery. UAVs are commonly used to produce 3D models of rivers, via SfM or LiDAR. In rivers, these techniques are challenged by water, which may require a bathymetry correction to derive subsurface topography, although turbulence and unclear water can make this impossible and both are common in boulder-bed streams. Green LiDAR can also be used to sense topography below the water surface, but with similar constraints (Kastdalen et al., 2024). Alternatively, UAV are often used in parallel with specialised bathymetric surveying techniques like Acoustic Doppler Current Profilers or Sonar (e.g. Koutalakis & Zaimes, 2022), but these are typically suited to deeper rivers. Many boulder-bed rivers are likely to be too shallow to be optimal for many of these techniques but too turbid or turbulent for UAV and LiDAR. Consequently, collecting high-resolution 3D surfaces below water and between overlapping boulders usually requires some degree of field data collection (Rusnák et al., 2018), resulting in many of the disadvantages of field surveys (Table 3).

Nevertheless, in streams where 3D topography is available this will negate many of the constraints of the technique over field surveys, since multiple axes of particles can be measured and boulders can be identified below the water surface. At shallow sites, it is also possible that the shape and size of boulders can be inferred from the portions protruding above the water surface, but this will vary based on boulder characteristics, likely on a site-by-site or even individual boulder basis. Furthermore, increasingly, earth science research is working towards automated identification of boulders and other features of river environments (e.g. Rivas Casado et al., 2017), which may be possible both from 3D models and orthoimagery. Our findings suggest that these studies require a thorough investigation of the implications of their assumptions. Our findings would also apply to satellite imagery, which offers unparalleled spatial and temporal scales for environmental analysis (Tomsett & Leyland, 2019).

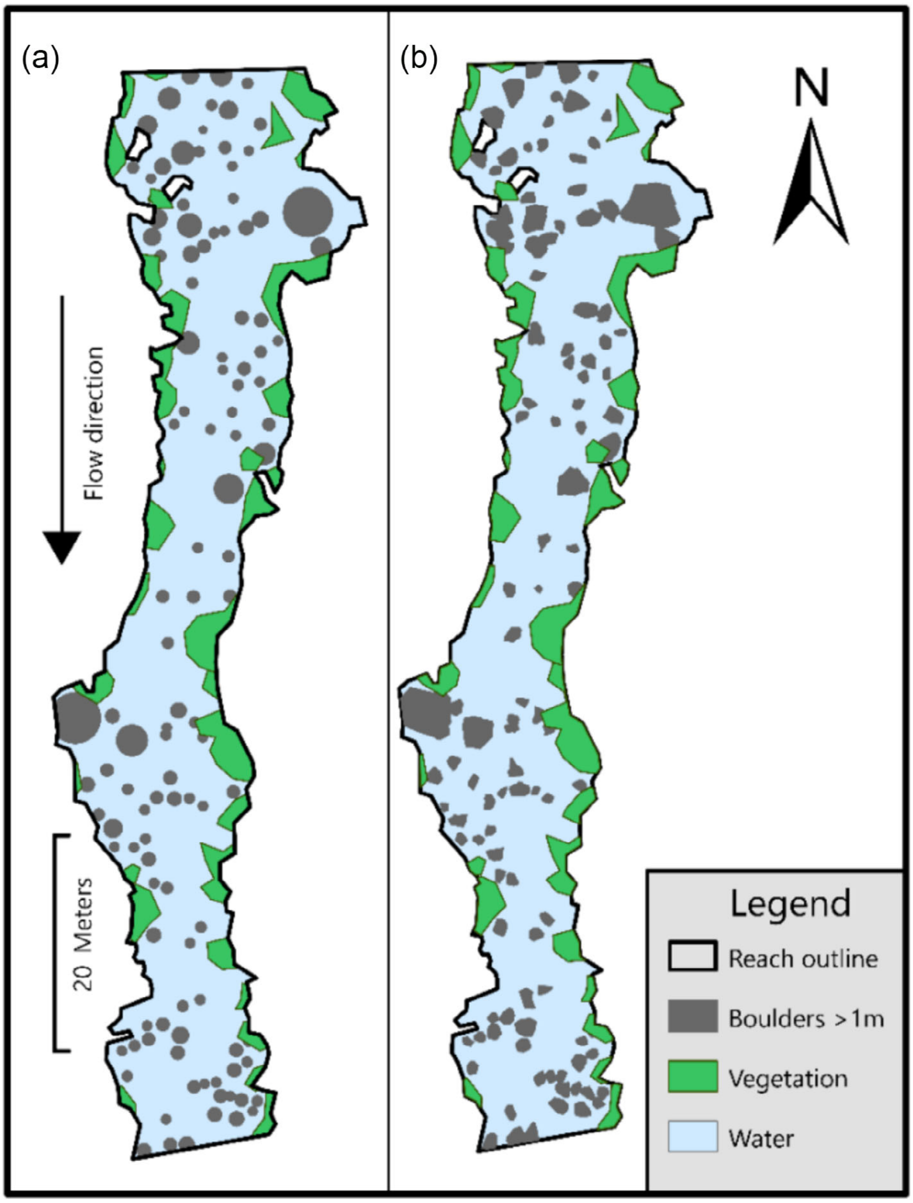

FIGURE 10 (a) Boulders were mapped as circles in this study to allow comparison between field and UAV data. (b) At one site (Reach 4), we compared this method to a measure of aerial coverage (including all visible boulders above and below water). Mapping as circles with diameter of b-axis, captured 86% coverage of the total horizontal surface area covered by boulders.

5 | CONCLUSIONS

New technologies continuously increase our ability to describe earth surface processes in more detail and at larger spatial and temporal scales. Aerial imagery collected by UAV provides a powerful tool to assess river health and morphology. However, understanding the extent to which aerial imagery can replace or complement field measurements, and in particular, whether they capture the same variables and processes as field surveys is important. We aimed to compare measurements of river boulders from aerial imagery collected by UAVs to direct measurements in the field to understand how and why techniques might differ.

We found that UAV boulder measurements resulted in consistently lower values for boulder density, coverage and size (34%, 32% and 7% less, respectively). However, there was a strong association across the sites between the boulder metrics measured in the field and with UAV. Studies estimating boulders from aerial imagery likely underestimate the amount of boulder compared to field surveys. However, in a relative sense, the degree of boulder influence can be effectively captured by UAV surveys.

We found that channel depth was a strong control on the difference between UAV and field measurements. Therefore, we caution use of aerial imagery for studies where spatial or temporal bias due to water coverage could influence results. Such bias in effectiveness of boulder identification with depth is also likely present with field measurements but less so since boulders can still be identified under the water. In general, remote sensing studies often have invisible areas (under trees and under water), and assessing how much missing data is acceptable is important. Overall, if the limitations of UAV-derived orthoimagery can be accepted, they provide a cost-effective and efficient alternative to field surveys.

AUTHOR CONTRIBUTIONS

Conceptualization: Richard J. Mason. *Funding acquisition*: Lina E. Polvi. *Methodology (including methodological development)*: Christopher Wård and Richard J. Mason. *Investigation (e.g. data collection)*: Christopher Wård, Richard J. Mason and Ricardo Carrillo. *Resources (provision of data, etc.)*: Richard J. Mason and Lina E. Polvi. *Software (its provision and development) and supervision*: Richard J. Mason and Lina E. Polvi. *Writing—initial draft*: Christopher Wård and Richard J. Mason.

Writing—reviewing and editing: Richard J. Mason, Ricardo Carrillo and Lina E. Polvi.

ACKNOWLEDGEMENTS

A big thank you to Jens Andersson and Mariana Busarello for their help in the field and to Pija Lapajne for assistance with geospatial analysis. Thank you to Birgitta Malm-Renöfält and Åsa Widén for their help with UAV surveying. Thank you to two anonymous reviewers whose suggestions improved the article. Funding for this research was provided by a R&D-project grant (2014-00484) for young research leaders from the Swedish Research Council Formas and a grant from the Swedish Agency for Marine and Water Management, both to LEP.

DATA AVAILABILITY STATEMENT

Data are available from the authors upon reasonable request.

ORCID

Richard J. Mason https://orcid.org/0000-0002-4571-7393
Ricardo Carrillo https://orcid.org/0000-0001-5110-6268
Lina E. Polvi https://orcid.org/0000-0002-6075-9890

REFERENCES

Acharya, B.S., Bhandari, M., Bandini, F., Pizarro, A., Perks, M., Joshi, D.R., et al. (2021) Unmanned aerial vehicles in hydrology and water management: Applications, challenges, and perspectives. *Water Resources Research*, 57(11), e2021WR029925. Available from: https://doi.org/10.1029/2021WR029925

Bangen, S.G., Wheaton, J.M., Bouwes, N., Bouwes, B. & Jordan, C. (2014) A methodological intercomparison of topographic survey techniques for characterizing wadeable streams and rivers. *Geomorphology*, 206, 343–361. Available from: https://doi.org/10.1016/j.geomorph.2013.10.010

Brasington, J., Vericat, D. & Rychkov, I. (2012) Modeling river bed morphology, roughness, and surface sedimentology using high resolution terrestrial laser scanning. *Water Resources Research*, 48(11), W11519. Available from: https://doi.org/10.1029/2012WR012223

Buscombe, D., Rubin, D.M. & Warrick, J.A. (2010) A universal approximation of grain size from images of noncohesive sediment. *Journal of Geophysical Research: Earth Surface*, 115(F2), F02015. Available from: https://doi.org/10.1029/2009jf001477

Carbonneau, P.E., Lane, S.N. & Bergeron, N.E. (2004) Catchment-scale mapping of surface grain size in gravel bed rivers using airborne digital imagery. *Water Resources Research*, 40(7), W07202. Available from: https://doi.org/10.1029/2003WR002759

Causon Deguara, J., Gauci, R. & Inkpen, R. (2023) Monitoring coastal erosion using remote images: Comparison between physically and remotely acquired data on a limestone coast. *Remote Sensing*, 15(1), 36. Available from: https://doi.org/10.3390/rs15010036

Chen, Y., DiBiase, R.A., McCarroll, N. & Liu, X. (2019) Quantifying flow resistance in mountain streams using computational fluid dynamics modeling over structure-from-motion photogrammetry-derived microtopography. *Earth Surface Processes and Landforms*, 44(10), 1973–1987. Available from: https://doi.org/10.1002/esp.4624

Church, M.A., McLean, D.G. & Wolcott, J.F. (1987) In: Thorne, C.R., Bathurst, J.C. & Hey, R.D. (Eds.) *River bed gravels: Sampling and analysis*. Chichester: Wiley, pp. 43–85.

Finnegan, N.J., Broudy, K.N., Nereson, A.L., Roering, J.J., Handwerger, A.L. & Bennett, G. (2019) River channel width controls blocking by slow-moving landslides in California's Franciscan mélange. *Earth Surface Dynamics*, 7(3), 879–894. Available from: https://doi.org/10.5194/esurf-7-879-2019

Golpira, A., Baki, A.B.M., Ghamry, H., Katopodis, C., Withers, J. & Minkoff, D. (2022) An experimental study: Effects of boulder placement on hydraulic metrics of instream habitat complexity. *Scientific Reports*, 12(1), 13156. Available from: https://doi.org/10.1038/s41598-022-17281-1

Gómez-Gutiérrez, Á., Sánchez-Fernández, M., de Sanjosé-Blasco, J.J., Gudino-Elizondo, N. & Lavado-Contador, F. (2024) Is it possible to generate accurate 3D point clouds with UAS-LIDAR and UAS-RGB photogrammetry without GCPs? A case study on a beach and rocky cliff. *Landscape Ecology*, 39(11), 191. Available from: https://doi.org/10.1007/s10980-024-01984-z

Graham, D.J., Reid, I. & Rice, S.P. (2005) Automated sizing of coarse-grained sediments: Image-processing procedures. *Mathematical Geology*, 37(1), 1–28. Available from: https://doi.org/10.1007/s11004-005-8745-x

Green, J.C. (2003) The precision of sampling grain-size percentiles using the Wolman method. *Earth Surface Processes and Landforms*, 28(9), 979–991. Available from: https://doi.org/10.1002/esp.513

Hancock, S., McGrath, C., Lowe, C., Davenport, I. & Woodhouse, I. (2021) Requirements for a global lidar system: Spaceborne lidar with wall-to-wall coverage. *Royal Society Open Science*, 8(12), 211166. Available from: https://doi.org/10.1098/rsos.211166

Hodge, R., Brasington, J. & Richards, K. (2009) Analysing laser-scanned digital terrain models of gravel bed surfaces: Linking morphology to sediment transport processes and hydraulics. *Sedimentology*, 56(7), 2024–2043. Available from: https://doi.org/10.1111/j.1365-3091.2009.01068.x

James, M.R., Chandler, J.H., Eltner, A., Fraser, C., Miller, P.E., Mills, J.P., et al. (2019) Guidelines on the use of structure-from-motion photogrammetry in geomorphic research. *Earth Surface Processes and Landforms*, 44(10), 2081–2084. Available from: https://doi.org/10.1002/esp.4637

Kastdalen, L., Stickler, M., Malmquist, C. & Heggenes, J. (2024) Evaluating methods for measuring in-river bathymetry: Remote sensing green LIDAR provides high-resolution channel bed topography limited by water penetration capability. *River Research and Applications*, 40(4), 467–482. Available from: https://doi.org/10.1002/rra.4245

Korpak, J. (2017) Human impact on mountain streams and rivers. In: *Open channel hydraulics, river hydraulic structures and fluvial geomorphology*. Boca Raton: CRC Press, pp. 400–435 https://doi.org/10.1201/9781315120584-21

Koutalakis, P. & Zaimes, G.N. (2022) River flow measurements utilizing UAV-based surface velocimetry and bathymetry coupled with sonar. *Hydrology*, 9(8) Article 8, 148. Available from: https://doi.org/10.3390/hydrology9080148

Kritzberg, E.S., Hasselquist, E.M., Škerlep, M., Löfgren, S., Olsson, O., Stadmark, J., et al. (2020) Browning of freshwaters: Consequences to ecosystem services, underlying drivers, and potential mitigation measures. *Ambio*, 49(2), 375–390. Available from: https://doi.org/10.1007/s13280-019-01227-5

Lang, N., Irniger, A., Rozniak, A., Hunziker, R., Wegner, J.D. & Schindler, K. (2021) GRAINet: Mapping grain size distributions in river beds from UAV images with convolutional neural networks. *Hydrology and Earth System Sciences*, 25(5), 2567–2597. Available from: https://doi.org/10.5194/hess-25-2567-2021

Langhammer, J. (2019) Uav monitoring of stream restorations. *Hydrology*, 6(2), 29. Available from: https://doi.org/10.3390/hydrology6020029

Lee, A.J. & Ferguson, R.I. (2002) Velocity and flow resistance in step-pool streams. *Geomorphology*, 46(1–2), 59–71. Available from: https://doi.org/10.1016/S0169-555X(02)00054-5

Mangold, N., Gupta, S., Gasnault, O., Dromart, G., Tarnas, J.D., Sholes, S.F., et al. (2021) Perseverance rover reveals an ancient delta-lake system and flood deposits at Jezero crater, Mars. *Science*, 374(6568), 711–717. Available from: https://doi.org/10.1126/science.abl4051

Marchetti, G., Bizzi, S., Belletti, B., Lastoria, B., Comiti, F. & Carbonneau, P.E. (2022) Mapping riverbed sediment size from Sentinel-2 satellite data. *Earth Surface Processes and Landforms*, 47(10), 2544–2559. Available from: https://doi.org/10.1002/esp.5394

Mason, R.J. & Polvi, L.E. (2023) Unravelling fluvial versus glacial legacy controls on boulder-bed river geomorphology for semi-alluvial rivers in Fennoscandia. *Earth Surface Processes and Landforms*, 48(14), 2900–2919. Available from: https://doi.org/10.1002/esp.5666

Mason, R.J. & Polvi, L.E. (2024) How big is a boulder? The importance of boulder definition choice in earth science research and river management. *Earth Surface Processes and Landforms*, 49(9), 2840–2854. Available from: https://doi.org/10.1002/esp.5861

Mohren, J. & Schulze, M. (2024) Automated cleaning of tie point clouds following USGS guidelines in Agisoft Metashape professional (ver. 2.1. 0). *MethodsX*, 12, 102679. Available from: https://doi.org/10.1016/j.mex.2024.102679

Montgomery, D.R. & Buffington, J.M. (1997) Channel-reach morphology in mountain drainage basins. *Geological Society of America Bulletin*, 109(5), 596–611.

Nativ, R., Turowski, J.M., Goren, L., Laronne, J.B. & Shyu, J.B.H. (2022) Influence of rarely mobile boulders on channel width and slope: Theory and field application. *Journal of Geophysical Research: Earth Surface*, 127(9), e2021JF006537. Available from: https://doi.org/10.1029/2021JF006537

Nikolakopoulos, K.G., Kyriou, A., Koukouvelas, I.K., Tomaras, N. & Lyros, E. (2023) UAV, GNSS, and InSAR data analyses for landslide monitoring in a Mountainous Village in Western Greece. *Remote Sensing*, 15(11), 2870. Available from: https://doi.org/10.3390/rs15112870

Nilsson, C., Lepori, F., Malmqvist, B., Törnlund, E., Hjerdt, N., Helfield, J.M., et al. (2005) Forecasting environmental responses to restoration of rivers used as log floatways: An interdisciplinary challenge. *Ecosystems*, 8(7), 779–800. Available from: https://doi.org/10.1007/s10021-005-0030-9

Nilsson, C., Polvi, L.E., Gardeström, J., Hasselquist, E.M., Lind, L. & Sarneel, J.M. (2015) Riparian and in-stream restoration of boreal streams and rivers: Success or failure?: Success or failure of stream restoration. *Ecohydrology*, 8(5), 753–764. Available from: https://doi.org/10.1002/eco.1480

Papanicolaou, A.N., (Thanos), Tsakiris, A.G., Wyssmann, M.A. & Kramer, C.M. (2018) Boulder array effects on bedload pulses and depositional patches. *Journal of Geophysical Research: Earth Surface*, 123(11), 2925–2953. Available from: https://doi.org/10.1029/2018JF004753

Pérez-Alberti, A. & Trenhaile, A.S. (2015) An initial evaluation of drone-based monitoring of boulder beaches in Galicia, North-Western Spain. *Earth Surface Processes and Landforms*, 40(1), 105–111. Available from: https://doi.org/10.1002/esp.3654

Resop, J.P., Kozarek, J.L. & Hession, W.C. (2012) Terrestrial laser scanning for delineating in-stream boulders and quantifying habitat complexity measures. *Photogrammetric Engineering & Remote Sensing*, 78(4), 363–371. Available from: https://doi.org/10.14358/PERS.78.4.363

Rivas Casado, M., González, R.B., Ortega, J.F., Leinster, P. & Wright, R. (2017) Towards a transferable UAV-based framework for river hydromorphological characterization. *Sensors (Basel)*, 17(10), 2210. Available from: https://doi.org/10.3390/s17102210

Rusnák, M., Sládek, J., Kidová, A. & Lehotský, M. (2018) Template for high-resolution river landscape mapping using UAV technology. *Measurement*, 115, 139–151. Available from: https://doi.org/10.1016/j.measurement.2017.10.023

Rust, B.R. (1972) Pebble orientation in fluvial sediments. *Journal of Sedimentary Research*, 42(2), 384–388. Available from: https://doi.org/10.1306/74d7255e-2b21-11d7-8648000102c1865d

Sakamoto, M. & Gomez, C. (2019) Assessment of UAV-based photogrammetry in lahar valleys to estimate boulder potential hazards-field experiment at Unzen volcano (Japan). *International Journal of Innovative Technology and Exploring Engineering (IJITEE)*, 8(6S3), 567–573.

Siewert, M.B. & Olofsson, J. (2020) Scale-dependency of Arctic ecosystem properties revealed by UAV. *Environmental Research Letters*, 15(9), 094030. Available from: https://doi.org/10.1088/1748-9326/aba20b

Tomsett, C. & Leyland, J. (2019) Remote sensing of river corridors: A review of current trends and future directions. *River Research and Applications*, 35(7), 779–803. Available from: https://doi.org/10.1002/rra.3479

Törnlund, E. & Östlund, L. (2006) Mobility without wheels: The economy and ecology of timber floating in Sweden, 1850–1980. *The Journal of Transport History*, 27(1), 48–70. Available from: https://doi.org/10.7227/TJTH.27.1.5

Viles, H. (2016) Technology and geomorphology: Are improvements in data collection techniques transforming geomorphic science? *Geomorphology*, 270, 121–133. Available from: https://doi.org/10.1016/j.geomorph.2016.07.011

Wiener, J.S. & Pasternack, G.B. (2022) Scale dependent spatial structuring of mountain river large bed elements maximizes flow resistance. *Geomorphology*, 416, 108431. Available from: https://doi.org/10.1016/j.geomorph.2022.108431

Williams, R.D., Bangen, S., Gillies, E., Kramer, N., Moir, H. & Wheaton, J. (2020) Let the river erode! Enabling lateral migration increases geomorphic unit diversity. *Science of the Total Environment*, 715, 136817. Available from: https://doi.org/10.1016/j.scitotenv.2020.136817

Woellner, R. & Wagner, T.C. (2019) Saving species, time and money: Application of unmanned aerial vehicles (UAVs) for monitoring of an endangered alpine river specialist in a small nature reserve. *Biological Conservation*, 233, 162–175. Available from: https://doi.org/10.1016/j.biocon.2019.02.037

Wohl, E. (2019) Forgotten legacies: Understanding and mitigating historical human alterations of river corridors. *Water Resources Research*, 55(7), 5181–5201. Available from: https://doi.org/10.1029/2018WR024433

Woodget, A.S., Austrums, R., Maddock, I.P. & Habit, E. (2017) Drones and digital photogrammetry: From classifications to continuums for monitoring river habitat and hydromorphology. *WIREs Water*, 4(4), e1222. Available from: https://doi.org/10.1002/wat2.1222

Woodget, A.S., Carbonneau, P.E., Visser, F. & Maddock, I.P. (2015) Quantifying submerged fluvial topography using hyperspatial resolution UAS imagery and structure from motion photogrammetry. *Earth Surface Processes and Landforms*, 40(1), 47–64. Available from: https://doi.org/10.1002/esp.3613

How to cite this article: Wård, C., Mason, R.J., Carrillo, R. & Polvi, L.E. (2025) Potential and constraints of uncrewed aerial vehicle orthoimagery for rivers: A direct comparison with field measurements for mapping boulders. *Earth Surface Processes and Landforms*, 50(8), e70106. Available from: https://doi.org/10.1002/esp.70106